Thermocapillary and electrohydrodynamic effects on the stability of dynamic contact lines

Devin T. Conroy,[1] Leonardo Espín,[2] Omar K. Matar,[1] and Satish Kumar[2,*]

[1]*Department of Chemical Engineering, Imperial College London, London SW7 2AZ, United Kingdom*
[2]*Department of Chemical Engineering and Materials Science, University of Minnesota,
Minneapolis, Minnesota 55455, USA*

Motivated by the need to understand how external fields influence the stability of dynamic contact lines, the linear stability of gravity-driven spreading of a thin liquid film in the presence of electric and temperature fields is studied. The film is confined from below by a flat substrate and from above by an air gap and another flat substrate. An electrostatic potential difference or temperature difference can be applied between the two substrates and the liquid is taken to be a perfect dielectric whose surface tension decreases linearly with temperature. Traveling-wave solutions are found for the film profile, and both electric and temperature fields influence the height of the capillary ridge of liquid that forms near the advancing contact line. The linear stability analysis shows that electric fields destabilize the film front to transverse perturbations and that temperature fields can either stabilize or destabilize the front, depending on the direction of the temperature gradient. An energy analysis reveals that the electric field in the capillary ridge is most responsible for the enhancement of the perturbation growth. For the case of temperature fields, the perturbed temperature gradients are the dominant mechanism through which the perturbation in film height is affected.

I. INTRODUCTION

Thin liquid films with dynamic contact lines driven by body forces arise in many technological applications, ranging from the operation of microfabricated devices [1] to the coating of medical devices [2] and beyond. When a liquid film with a contact line is driven by gravity, a ridge of liquid known as the capillary ridge rises above the film in the upstream region. In these situations, traveling-wave solutions for the liquid profile can be calculated which show the quasisteady shape of the capillary ridge [3–5]. The capillary ridge has been shown to destabilize the front of the liquid film to disturbances in the spanwise direction which can grow into rivulets or fingers and negatively impact the uniformity of a liquid coating [6,7]. It is thus of interest to investigate methods for controlling the growth of the capillary ridge and stabilizing the contact line to spanwise disturbances.

Electric fields [8–10] and temperature gradients [11,12] can be used to control liquids at small length scales and may have a significant influence on the stability of contact lines of driven liquid films. Electric fields are already present in gravity-driven flows which arise in electrospray coating [13] where uniform films are typically desired, and temperature gradients can be used to drive and influence spreading films [14,15]. Combinations of these can further affect the stability of thin films and the motion of droplets [12,16].

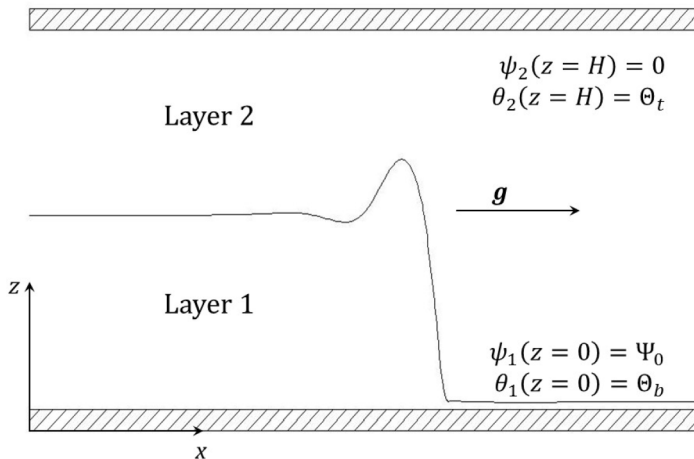*Corresponding author: kumar030@umn.edu

FIG. 1. Schematic of problem geometry. The x and z axes are shown, while the y axis points into the page. The electrostatic potential and temperature in each layer are denoted by ψ_i and θ_i, respectively.

There has been a considerable amount of prior work examining the influence of electric and temperature fields on the behavior of thin liquid films and droplets; reviews can be found in Refs. [7,17–21]. Electric fields affect interface shapes through charge polarization, which modifies the normal stress balance. If free charge is present at interfaces, then tangential stresses can arise. Electric fields can also modify contact angles. Temperature fields influence interface shapes primarily through thermocapillary stresses. The resulting tangential forces along the interface tend to drag liquid to regions of lower temperature (higher surface tension) from regions of higher temperature (lower surface tension).

Although methods for stabilizing dynamic contact lines could be instrumental in producing more uniform coatings, little is understood about how electric and temperature fields might affect the stability of the film front. Tseluiko *et al.* [22,23] have shown that electric fields affect capillary-ridge growth in gravity-driven film flows over topography where there are no contact lines. Kataoka and Troian [14] observed the fingering instability in thermally driven films, while Klentzman and Ajaev [15] showed that Marangoni effects can promote the fingering instability in gravity-driven films when heated from below. However, the effects of electric fields or cooling the liquid from below on the spanwise stability of gravity-driven films with contact lines have not been studied.

Here we examine the gravity-driven flow of a constant-flux liquid film in the presence of normal electric and temperature fields. We apply the lubrication approximation and obtain an evolution equation for interface height. We first study electrohydrodynamic (EHD) and thermocapillary (TC) effects on the traveling-wave solutions to the height evolution equation. We then conduct a linear stability analysis of the traveling-wave solutions and characterize the effects of the electric and temperature fields on the stability of the dynamic contact line. An energy analysis is performed to gain insight into the mechanisms behind the EHD and TC effects on the contact-line instability. Our results demonstrate that while electric fields enhance the fingering instability, temperature gradients can be used to suppress the fingering instability and thus could be of use in efforts to generate uniform coatings.

II. PROBLEM FORMULATION

We consider a constant flux of liquid being driven down a vertical substrate by gravity (Fig. 1). An electrode is suspended above and parallel to the substrate at a height H. An electrostatic potential of magnitude Ψ_0 is applied at the substrate (assumed to be a perfect conductor) while the top electrode is grounded. We assume the substrate and electrode are held at constant temperatures Θ_b and Θ_t,

respectively. The parallel configuration of the electrodes provides a good starting point for gaining physical understanding by allowing us to invoke the lubrication approximation when the electrode spacing H is small compared to the horizontal length scale L (defined in Sec. II B). The liquid, layer 1, has viscosity η, density ρ, and surface tension γ. We assume the liquid is a perfect dielectric with dielectric constant ε_1. The air layer above the liquid is referred to as layer 2 and assumed to have small enough viscosity and density such that its flow can be neglected.

A. Governing equations

We use the Navier-Stokes equations to describe the liquid flow in layer 1,

$$\nabla \cdot \mathbf{v} = 0, \tag{1}$$

$$\rho \frac{D\mathbf{v}}{Dt} = \nabla \cdot \mathbf{T}_1 + \rho g \mathbf{e}_x, \tag{2}$$

where g is the constant gravitational acceleration, $\mathbf{v} = (v_x, \ v_y, \ v_z)$ is the velocity vector, and $\mathbf{T}_1$ is the total stress tensor of the liquid, defined as

$$\mathbf{T}_1 = -p_1 \mathbf{I} + \tfrac{1}{2} \eta [\nabla \mathbf{v} + (\nabla \mathbf{v})^T] + \mathbf{M}_1, \tag{3}$$

where $\mathbf{I}$ is the identity tensor, p_1 is the liquid pressure, and $\mathbf{M}_1$ is the Maxwell stress tensor which is defined later in this section. We ignore the flow in the air layer and thus the stress tensor in the air is the sum of the pressure and Maxwell stress tensor, given by

$$\mathbf{T}_2 = -p_2 \mathbf{I} + \mathbf{M}_2, \tag{4}$$

where p_2 is the pressure in the air.

We let $h(x, y, t)$ denote the location of the liquid-air interface, so from the normal stress balance we have, at $z = h(x, y, t)$,

$$\|\mathbf{n} \cdot \mathbf{T}_i \cdot \mathbf{n}\| = \kappa \gamma, \tag{5}$$

where $\mathbf{n}$ is a vector normal to the interface pointing into layer 2, κ is the mean curvature of the interface, and $\|f_i\| = f_2 - f_1$ for a given function f_i. The tangential stress balances state that at $z = h(x, y, t)$,

$$\|\mathbf{n} \cdot \mathbf{T}_i \cdot \mathbf{t}\| = -\nabla_S \gamma \cdot \mathbf{t}, \tag{6}$$

where $\mathbf{t}$ represents two vectors that are tangent to the interface and ∇_S is the surface gradient operator.

We also impose the no-slip and no-penetration conditions at the substrate,

$$\mathbf{v}(z = 0) = 0. \tag{7}$$

The interface position is governed by the kinematic condition

$$\frac{\partial h}{\partial t} = -\nabla \cdot (h\mathbf{v}). \tag{8}$$

The electric field is described by Maxwell's equations, simplified for the case where magnetic effects are negligible (i.e., the electrostatic limit). In this case the electric field $\mathbf{E}$ is irrotational and can be defined in terms of a potential as

$$\mathbf{E}_i = -\nabla \psi_i, \tag{9}$$

where ψ_i is the electrostatic potential. Ignoring charges in both fluids, the potential in each layer is governed by the Laplace equation

$$\nabla^2 \psi_i = 0 \tag{10}$$

and the boundary conditions

$$\psi_1(z = 0) = \Psi_0, \tag{11}$$

$$\psi_2(z = H) = 0, \tag{12}$$

$$\psi_1(z = h) = \psi_2(z = h). \tag{13}$$

We consider only perfect dielectric (i.e., nonconductive) liquids, so the jump in the normal component of the electric field is [24]

$$\|\varepsilon_i \varepsilon_0 \mathbf{E}_i\| \cdot \mathbf{n} = 0, \tag{14}$$

where ε_0 is the permittivity of free space. We set the permittivity of the air layer as $\varepsilon_2 = 1$ and define the permittivity of the liquid layer as $\varepsilon_1 = \varepsilon$. As noted above, the interaction between the electric field and the fluids is described by the Maxwell stress tensor, defined in each layer i as

$$\mathbf{M}_i = \varepsilon_i \varepsilon_0 \big[\mathbf{E}_i \mathbf{E}_i - \tfrac{1}{2}(\mathbf{E}_i \cdot \mathbf{E}_i)\mathbf{I}\big]. \tag{15}$$

To model the temperature field θ, we apply the energy conservation equation in both layers,

$$\rho_i c_i \frac{D\theta_i}{Dt} = k_i \nabla^2 \theta_i, \tag{16}$$

where ρ_i, c_i, and k_i denote the density, specific heat, and thermal conductivity of layer i, respectively. Consistent with earlier studies (on problems without dynamic contact lines) [12,25,26] that use similar geometries, we assume that the effects of thermal convection are negligible, so the boundary conditions are

$$\theta_1(z = 0) = \Theta_b, \tag{17}$$

$$\theta_2(z = H) = \Theta_t, \tag{18}$$

$$\theta_1(z = h) = \theta_2(z = h), \tag{19}$$

$$\|k_i \boldsymbol{\nabla} \theta_i\| \cdot \mathbf{n} = 0 \quad \text{at } z = h. \tag{20}$$

It is assumed that the liquid surface tension decreases linearly with temperature so that $\gamma(\theta) = \gamma_R + \gamma_\theta(\theta - \Theta_R)$, where γ_R is a reference surface tension at temperature Θ_R and θ is the temperature at the interface. Here γ_θ is a constant, with units of surface tension divided by temperature, representing the slope of γ with respect to θ and is a measure of the deviation of the surface tension from the reference value γ_R. In addition, we will assume that $\gamma_R \gg |\gamma_\theta \Delta\Theta|$ so that we can ignore surface tension variations in the normal stress balance.

By imposing the no-slip condition and thus immobilizing the liquid in contact with the solid surface, the advancing contact line is also fixed in place. To resolve this issue, we follow a number of earlier studies [5,6,27–29] and assume that a thin precursor film of thickness b is present along the entire substrate. The contact line then becomes an *apparent* contact line with no substrate-air contact, which allows us to apply the no-slip condition without restricting the spreading of the film. Also, in the precursor-film model the viscous liquid is continuous all along the substrate, so the interfacial conditions for the electric field and temperature given above are applied all along the liquid-air interface. An alternative approach is to incorporate an explicit contact line along with a slip law and contact angle, but such a model is considerably more complex to implement numerically and is outside the scope of the current work.

Previous studies have shown that inclusion of a precursor film in models for the spreading of driven films leads to results that are qualitatively independent of b [6], although the exact rate at which the film front moves down the substrate is a function of b. Other methods for resolving the contact-line issue in spreading problems have included a slip condition [3] and numerical slip [30]. Again, all the methods yield results that are qualitatively similar, although the results differ quantitatively depending on the slip model chosen. In this paper we consider only the precursor-film model.

B. Scalings and lubrication approximation

We nondimensionalize the variables as

$$(v_x, v_y, v_z) = (U\bar{v}_x, U\bar{v}_y, W\bar{v}_z), \quad p_i = P\bar{p}_i, \quad \psi_i = \Psi_0\bar{\psi}_i,$$

$$(x, y, z) = (L\bar{x}, L\bar{y}, H\bar{z}), \quad t = T\bar{t}, \quad \bar{\theta}_i = (\theta_i - \Theta_t)/(\Theta_b - \Theta_t),$$

where variables with the overbar are dimensionless. The vertical length scale is chosen to be the electrode spacing H. From the continuity equation, the vertical velocity is scaled by $W = HU/L$. In the kinematic condition, we choose to scale time as $T = 3L/U$. We choose to scale horizontal velocity with $U = H^2\rho g/\eta$, which represents a balance of viscous and gravitational forces in the x component of the momentum equations. We scale pressure with the gravitational force, $P = L\rho g$. The horizontal length scale L is determined by a balance of surface tension and gravitational forces to be $L = (\gamma_R H/\rho g)^{1/3}$. A dimensionless electric force parameter arises in the normal stress balance, defined as the Coulomb number $\mathrm{Co} = \varepsilon_0\Psi_0^2/H^2L\rho g$. The Marangoni number comes from the tangential stress balances and is $\mathrm{Ma} = \gamma_\theta\Delta\Theta/HL\rho g$, with $\Delta\Theta = \Theta_b - \Theta_t$. The ratio of thermal conductivities is defined as $\kappa = k_2/k_1$.

The problem discussed here corresponds to a thin viscous dielectric film surrounded by an inviscid gas. A very thin precursor film is assumed to rest on an inclined perfectly conducting substrate (e.g., metal) and a constant flux of liquid flows along the substrate in the x direction. In the case of an oil film surrounded by air we have the following properties: $\epsilon = 2$, $\gamma_R = 0.3$ N/m, $\gamma_\theta = -1.5 \times 10^{-4}$ N/m °C, $\rho = 900$ kg/m^3, $\eta = 0.1$ N s/m^2, and $\kappa = 5$. Assuming that the electrode spacing $H = 5 \times 10^{-4}$ m, then $L = 1.2 \times 10^{-3}$ m, $\mathrm{Co}/\psi_0^2 = 3.3 \times 10^{-6}$, and $\mathrm{Ma}/\Delta\theta = 0.028$. For $\mathrm{Co} = 0.2$ and $\mathrm{Ma} = 0.1$, the voltage across the plates is $\psi = 245$ V and the temperature difference is $\Delta\theta = 3.5$ °C.

After nondimensionalization, we apply the lubrication approximation and expand each equation in terms of $H/L \ll 1$, keeping only the leading-order terms. We solve for the potential, temperature, and velocities in terms of z and $h(x, y, t)$ (now dropping the overbars for dimensionless terms).

C. Evolution equations

As is customary in previous constant-flux studies, we change coordinate systems to one that moves at a constant speed along with the contact line, $(x, y, z, t) \rightarrow (\xi, y, z, t)$, where $\xi = x - Ut$ (we solve for U in the next section). Then $h \rightarrow h(\xi, y, t)$ and $\nabla \rightarrow (\frac{\partial}{\partial\xi}, \frac{\partial}{\partial y})$. We solve for $\mathbf{v}$ and p_1 in terms of h, ψ, and θ using the lubrication forms of the Navier-Stokes equations (1) and (2) subject to boundary conditions (5)–(7) to obtain

$$v_x = \frac{1}{2}z^2\left(\frac{\partial p}{\partial\xi} - 1\right) + \mathrm{Ma}\theta_x z - hz\left(\frac{\partial p}{\partial\xi} - 1\right), \tag{21}$$

$$v_z = \frac{1}{2}z^2\frac{\partial p}{\partial y} + \mathrm{Ma}\theta_y z - hz\frac{\partial p}{\partial y}, \tag{22}$$

$$p_1 = -\nabla^2 h + \frac{\mathrm{Co}}{2}\varepsilon(1 - \varepsilon)c_5^2. \tag{23}$$

The electrostatic potential ψ is solved for using Eqs. (10)–(14) and the temperature θ is obtained using Eqs. (16)–(20). Finally, we can then express the kinematic condition (8) as an evolution equation for h,

$$\frac{\partial h}{\partial t} = U\frac{\partial h}{\partial\xi} - \nabla\cdot(h^3\nabla\nabla^2 h) - \frac{\partial h^3}{\partial\xi} + \frac{\mathrm{Co}}{2}\varepsilon(1 - \varepsilon)\nabla\cdot\left(h^3\nabla c_5^2\right) - \frac{3}{2}\mathrm{Ma}\nabla\cdot[h^2\nabla\theta(h)], \tag{24}$$

where

$$c_5 = \frac{1}{h(\varepsilon - 1) - \varepsilon} \tag{25}$$

and the interfacial temperature is

$$\theta(z = h) = \frac{h\kappa}{h(1 - \kappa) - 1} + 1. \tag{26}$$

III. TRAVELING-WAVE SOLUTIONS

As noted earlier, previous studies on constant-flux flows with dynamic contact lines have shown that it is possible to solve the height evolution equation to obtain traveling-wave solutions that describe the flow prior to any spanwise perturbations [3,5]. To recover a traveling-wave solution to Eq. (24), let us first assume that h is y independent and thus simplify Eq. (24) to

$$\frac{\partial h}{\partial t} = U\frac{\partial h}{\partial \xi} - \frac{\partial}{\partial \xi}\left(h^3\frac{\partial^3 h}{\partial \xi^3}\right) - \frac{\partial h^3}{\partial \xi} + \frac{\text{Co}}{2}\varepsilon(1 - \varepsilon)\frac{\partial}{\partial \xi}\left(h^3\frac{\partial c_5^2}{\partial \xi}\right) - \frac{3}{2}\text{Ma}\frac{\partial}{\partial \xi}\left(h^2\frac{\partial\theta(h)}{\partial \xi}\right). \tag{27}$$

We use the boundary conditions

$$h(0, t) = h_F, \tag{28}$$

$$h(L_\xi, t) = b, \tag{29}$$

$$\left.\frac{\partial h}{\partial \xi}\right|_{\xi=0} = \left.\frac{\partial h}{\partial \xi}\right|_{\xi=L_\xi} = 0, \tag{30}$$

where our domain runs from $\xi = 0$ to $\xi = L_\xi$. The precursor-film thickness b is fixed in this case and the advancing front of height h_f essentially displaces the prewetted film. Ahead of the front a depression forms in the precursor film followed by a wavy structure that decays downstream. The thickness of the film affects this structure, but numerically it is not practical to take the limit of a zero film thickness, so we use a finite value of b such that $h_f \gg b$. Since the precursor film is thin, within this region $c_5 \sim -1/\epsilon$ and $\theta \sim 1$, which are constants. The variables c_5 and θ represent the influence of electrostatic and thermal effects, respectively, and because they approach constant values in the precursor-film region, their derivatives in that region are approximately zero. This suggests that electrostatic and thermal effects do not play a significant role in the precursor-film region [cf. Eq. (27)].

By assuming $\partial h/\partial t = 0$ and applying boundary conditions (28)–(30), Eq. (27) returns a steady-state solution for the interface height which we denote by $h_0(\xi)$. We make the substitution $h(\xi, t) \rightarrow h_0(\xi)$ in Eq. (27) and follow the same procedure as in Ref. [31] to convert Eq. (27) into the ordinary differential equation for $h_0(\xi)$,

$$0 = Uh_0 - h_0^3\frac{d^3 h_0}{d\xi^3} - h_0^3 + \frac{\text{Co}}{2}\varepsilon(1 - \varepsilon)h_0^3\frac{dc_{5,0}^2}{d\xi} - \frac{3}{2}\text{Ma}\,h_0^2\frac{dT_0}{d\xi} + d, \tag{31}$$

where d is a constant of integration and

$$c_{5,0} = 1/[h_0(\varepsilon - 1) - \varepsilon], \tag{32}$$

$$T_0 = (h_0 - 1)/[h_0(1 - \kappa) - 1]. \tag{33}$$

Application of the boundary conditions (28)–(30) (assuming uniform film thickness, uniform electrostatic potential, and uniform temperature at the ends of the domain) allows us to obtain

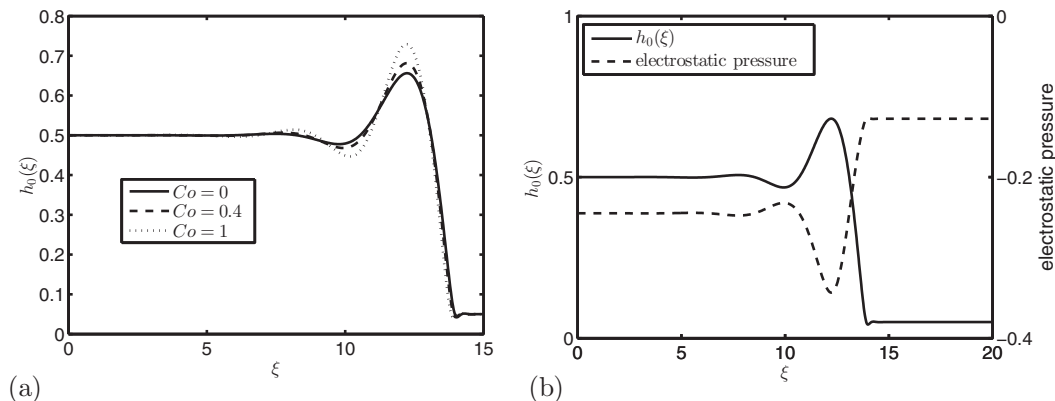$$U = b^2 + bh_F + h_F^2, \tag{34}$$

$$d = -bh_F(b + h_F). \tag{35}$$

FIG. 2. (a) Effect of electric field on the traveling wave. The values of other parameters are $\varepsilon = 2.5$ and $Ma = 0$. (b) Electrostatic pressure overlaid with the traveling-wave profile for $Co = 0.2$.

These expressions are equivalent to those found in previous studies, indicating that neither the presence of the electric field nor the temperature gradient appears to affect the velocity at which the film front moves down the substrate. However, Eq. (31) demonstrates that they do have an effect on the profile of the traveling wave through Co and Ma.

We solve for the traveling wave by specifying an initial condition for Eq. (27) and observing the long-time behavior of h. We use an initial condition similar to that in Ref. [32], a cubic polynomial with a contact line near the middle of the domain, given by

$$h(\xi, t = 0) = a_3\xi^3 + a_2\xi^2 + a_1\xi + a_0, \tag{36}$$

$$a_3 = 2(b - h_F)/(\xi_1 - \xi_2)^3, \tag{37}$$

$$a_2 = -3(b - h_F)(\xi_1 + \xi_2)/(\xi_1 - \xi_2)^3, \tag{38}$$

$$a_1 = 6(b - h_F)\xi_1\xi_2/(\xi_1 - \xi_2)^3, \tag{39}$$

$$a_0 = \left(-b\xi_1^3 + 3b\xi_1^2\xi_2 - 3h_F\xi_1\xi_2^2 + h_F\xi_2^3\right)/(\xi_1 - \xi_2)^3. \tag{40}$$

In our calculations, we typically choose $h_F = 0.5$, $b = 0.05$, and $L_\xi = 20$. The initial contact line is centered between ξ_1 and ξ_2, which are usually chosen to be $(\xi_1, \xi_2) = (14, 14.5)$. With this choice of parameters, the contact line settles well in the interior of our domain, minimizing the risk of edge effects. We use a fourth-order-accurate centered finite-difference method to discretize Eq. (27), and $h_0(\xi)$ is obtained from the solution to Eq. (27) at long times. For the time integration we use an implicit solver that is based on Gear's method, which allows us to take relatively large time steps.

We have examined the effect of the precursor-film thickness b on the steady-state interface profile. We find that the height of the capillary ridge increases as b decreases and the front speed increases as b increases [as expected from Eq. (34)]. Furthermore, as b decreases the interface profile appears to converge, but a finer grid resolution is required to obtain an accurate numerical solution. In all the cases of b investigated here, the interface profiles look qualitatively similar, and since we are principally interested in the electrohydrodynamic and thermocapillary effects on the evolution of a falling film and the formation of fingers, we fix the value of b in our study.

A. Electrohydrodynamic effects on the traveling wave

We begin by examining the effects of the electric field on the traveling wave. Figure 2(a) shows the film profile $h_0(\xi)$ near the contact-line region for several electric-field strengths. It is evident that

the electric field causes an increase in the height of the capillary ridge. Although we only present results for various values of Co, we note that an increase in the value of ε also enhances the growth of the capillary ridge.

The increase in capillary ridge height is due to electrohydrodynamic effects on the pressure. After nondimensionalizing and applying the lubrication approximation, the pressure is found from the normal stress balance ($p_1 = p$ and $p_2 = 0$) to be

$$p = -\nabla^2 h + \frac{\text{Co}}{2}\varepsilon(1-\varepsilon)c_5^2, \tag{41}$$

with the second term on the right-hand side representing the electrostatic contribution to the pressure, or electrostatic pressure. In Fig. 2(b) we can see that there is a minimum in the electrostatic pressure in the region of the capillary ridge. In the early stages of flow, the ridge forms at the apparent contact line due to viscous resistance to gravity-driven flow in the positive-ξ direction. Simultaneously, the electrostatic pressure acts to drive liquid from thinner regions of the film to thicker regions. Capillary pressure must then oppose both of these effects, which is achieved by the interface developing higher curvature. As Co increases (or similarly, as ε increases), so too does the electrostatic pressure, which results in a higher capillary ridge.

B. Thermocapillary effects on the traveling wave

The ability to control the direction of the temperature gradient allows for more control over the film profile than is possible with an electric field. By choosing either $\Theta_t > \Theta_b$ or $\Theta_t < \Theta_b$, the sign of Ma can be either positive or negative, respectively. Shown below is the dimensionless form of the tangential stress balance (6):

$$\left.\frac{\partial v_x}{\partial z}\right|_{z=h} = \text{Ma}\frac{\partial \theta(z=h)}{\partial \xi}. \tag{42}$$

Due to the way we nondimensionalize temperature, the direction of the tangential stress along the interface $h(\xi, t)$ is completely determined by the sign of Ma. This contrasts with the contribution to the pressure from the electric field, which depends on Co and $c_5[h(\xi, t)]^2$, both of which are invariant to the direction of the electric field. Since an increase in the conductivity ratio κ has the effect of reducing the magnitude of the temperature gradient, an increase in κ would lead to a reduction of thermocapillary effects.

Figure 3 compares the traveling-wave profile in the absence of a temperature gradient with the traveling-wave profile in the presence of two different temperature gradients. We see that Ma < 0, which corresponds to the top surface being cooled relative to the bottom surface, increases (albeit slightly) the height of the capillary ridge. In this case, a greater interfacial curvature is required for capillarity to counteract the combined effects of both the viscous resistance to gravity-driven flow and the upward shear stress generated from the temperature gradient along the liquid-air interface. Conversely, Ma > 0 slightly reduces the height of the capillary ridge as the thermocapillary stress now drives liquid down from the peak of the ridge.

IV. LINEAR STABILITY ANALYSIS

We now examine the stability of the traveling-wave solutions to spanwise perturbations. We consider normal mode perturbations h_1 to the quasisteady state h_0 using the expansion

$$h(\xi, y, t) = h_0(\xi) + \delta h_1(\xi, y, t), \tag{43}$$

where h_1 has the form $h_1 = g(\xi, t)e^{iqy}$, q denotes the wave number of the perturbation, and δ is a small parameter multiplying the $O(1)$ function h_1. Substitution of this expansion into Eq. (27) yields
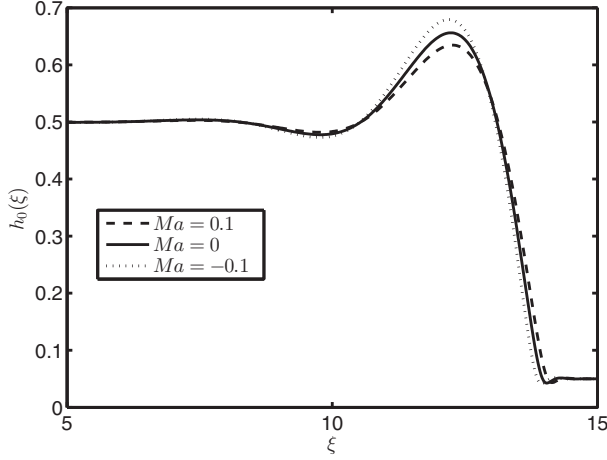
FIG. 3. Traveling-wave profiles for various values of Ma. The values of the other parameters are $\kappa = 5$ and Co = 0.

the partial differential equation for $g(\xi, t)$ to $O(\delta)$,

$$\frac{\partial g}{\partial t} = U\frac{\partial g}{\partial \xi} - \frac{\partial}{\partial \xi}\left(h_0^3\frac{\partial^3 g}{\partial \xi^3}\right) + \frac{\partial}{\partial \xi}\left(q^2 h_0^3\frac{\partial g}{\partial \xi}\right) - \frac{\partial}{\partial \xi}(3h_0^2 g) - \frac{\partial}{\partial \xi}\left(3h_0^2\frac{d^3 h_0}{d\xi^3}g\right) + q^2 h_0^3\frac{\partial^2 g}{\partial \xi^2} - q^4 h_0^3 g$$

$$+ \text{Co}\varepsilon(\varepsilon - 1)^2\frac{\partial}{\partial \xi}\left(h_0^3\frac{\partial}{\partial \xi}\left(c_{5,0}^3 g\right)\right) - \frac{3}{2}\text{Co}\varepsilon(\varepsilon - 1)\frac{\partial}{\partial \xi}\left[h_0^2\left(\frac{dc_{5,0}^2}{d\xi}\right)g\right] - q^2\text{Co}\varepsilon(\varepsilon - 1)^2 c_{5,0}^3 g$$

$$- \frac{3}{2}\text{Ma}\left[\frac{\partial}{\partial \xi}\left(2h_0\frac{dT_0}{d\xi}g\right) + \frac{\partial}{\partial \xi}\left(h_0^2\frac{\partial T_1}{\partial \xi}\right) - q^2 h_0^2 T_1\right], \tag{44}$$

where

$$T_1 = \{1/[h_0(1 - \kappa) - 1] - (1 - \kappa)(h_0 - 1)/[h_0(1 - \kappa) - 1]^2\}g. \tag{45}$$

For boundary conditions, we require $g(\xi, t)$ to decay to 0 as $\xi \to \pm\infty$. We then begin with a generic initial condition for g [we choose one period of a sine wave centered around $\xi = 10$, with $g(\xi, t) = 0$ everywhere else] and solve Eq. (44) numerically with a fourth-order-accurate centered finite-difference method. At long times, $\partial g/\partial t$ grows or decays exponentially, and a growth rate σ at a given q can be calculated from the L^2-norm of g [31]. This process is then repeated over a range of q values to obtain a dispersion relation.

A. Electrohydrodynamic effects on front stability

We first consider electrohydrodynamic effects on the stability of the film front in the absence of a temperature gradient, i.e., Co $\neq$ 0 and Ma = 0. Before exploring the full range of wave numbers, we analytically examine the low-q limit in a manner similar to that described in Ref. [31]. We assume g grows exponentially with t so that $g = \phi(\xi)e^{\sigma t}$, and then expand both σ and g as follows: $\sigma = \sigma_0 + q^2\sigma_1 + O(q^4)$ and $g = [\phi_0(\xi) + q^2\phi_1(\xi) + O(q^4)]e^{\sigma t}$. These expansions are then substituted into Eq. (44) and expressions for σ_0 and σ_1 are obtained. We find that for Co $\neq$ 0, $\sigma_0 = 0$ and the growth rate can be approximated to $O(q^2)$ by

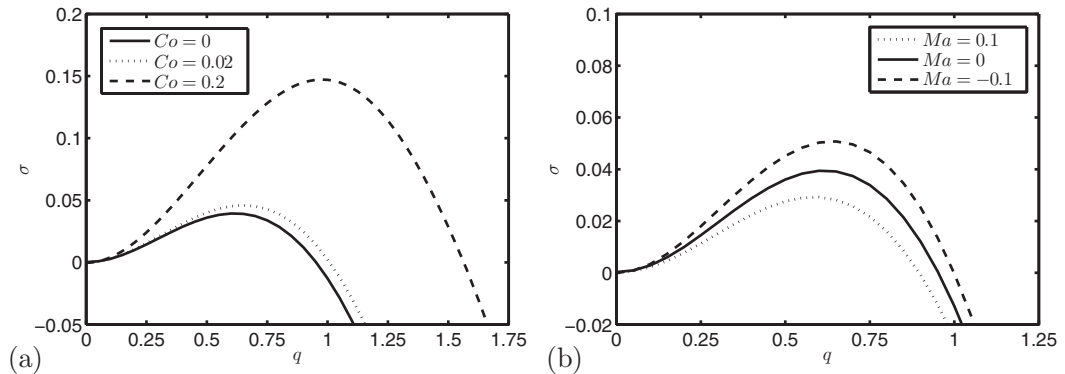$$\sigma \approx \frac{q^2}{h_F - b}\int_{-\infty}^{\infty}(h_0 - b)(h_0 - h_F)(h_0 + h_F + b)d\xi. \tag{46}$$

FIG. 4. (a) Dispersion relations showing electrohydrodynamic effects on front stability at various values of Co. The values of the other parameters are $\varepsilon = 2.5$ and $Ma = 0$. (b) Dispersion relations showing thermocapillary effects on front stability at various values of Ma. The values of the other parameters are $\kappa = 5$ and $Co = 0$.

This expression is identical to that obtained in the absence of an electric field, suggesting that in the low-q limit, the electric field only influences stability through its effect on the shape of the base state $h_0(\xi)$.

Figure 4(a) shows the growth rate plotted against the wave number calculated from Eq. (44) at various values of Co. The results for $Co = 0$ agree well with previous studies [3,6], with quantitative differences arising from differing initial conditions ($h_F = 0.5$ instead of 1 and $b = 0.05$ instead of 0.1 or 0.01). Although not shown here for brevity, results from the asymptotic formula (46) agree well with solutions of Eq. (44) at low q.

As shown in Fig. 4(a), the presence of an electric field increases both the most unstable wave number and maximum growth rate. The destabilization created by the electric field might be expected based on the results of Sec. III A, which show that the electric field increases the height of the capillary ridge. We look further into the mechanism for this destabilization in Sec. V.

B. Thermocapillary effects on front stability

We now consider thermocapillary effects on the stability of the film front in the absence of an electric field, i.e., $Ma \neq 0$ and $Co = 0$. We performed a low-q analysis of Eq. (44) for $Ma \neq 0$, but were unable to obtain an explicit expression for σ such as Eq. (46). Figure 4(b) shows the growth rate plotted against the wave number calculated from Eq. (44) at various values of Ma. Here we see that the effect of the temperature gradient on the instability is indicated by its effect on the capillary ridge. Temperature fields corresponding to $Ma < 0$ result in a higher capillary ridge and accordingly increase the growth rate and most unstable wave number. Likewise, $Ma > 0$ results in a lower capillary ridge and stabilization of the front, as seen by the reduction of both the growth rate and most unstable wave number. However, we note that in both cases the influence of the temperature gradient on the instability is quite large and thus is unlikely to be explained solely by the relatively minor increase in the height of the capillary ridge of the traveling-wave profile seen in Fig. 3. We discuss the mechanisms for these effects in more detail in Sec. V.

V. ENERGY ANALYSIS

In this section we perform an energy analysis similar to those done by Spaid and Homsy [3] and Tiwari *et al.* [33]. We can see from Eq. (44) that the time rate of change of g is the sum of 13 terms: seven which are present in the gravity-driven spreading problem [3], three which arise from

TABLE I. Terms of operator L in the stability problem along with their physical meanings.

Term No.	Term	Physical meaning
1	$U \frac{\partial g}{\partial \xi}$	flow in the ξ direction due to reference velocity
2	$-\frac{\partial}{\partial \xi}\left(h_0^3 \frac{\partial^3 g}{\partial \xi^3}\right)$	flow in the ξ direction due to ξ curvature
3	$\frac{\partial}{\partial \xi}\left(q^2 h_0^3 \frac{\partial g}{\partial \xi}\right)$	flow in the ξ direction due to y curvature
4	$-\frac{\partial}{\partial \xi}\left(3h_0^2 g\right)$	flow in the ξ direction due to gravity
5	$-\frac{\partial}{\partial \xi}\left(3h_0^2 \frac{d^3 h_0}{d\xi^3} g\right)$	flow in the ξ direction driven by the base-state pressure gradient
6	$q^2 h_0^3 \frac{\partial^2 g}{\partial \xi^2}$	flow in the y direction due to ξ curvature
7	$-q^4 h_0^3 g$	flow in the y direction due to y curvature
8	$\mathrm{Co}\varepsilon(\varepsilon-1)^2 \frac{\partial}{\partial \xi}\left(h_0^3 \frac{\partial}{\partial \xi}\left(c_{5,0}^3 g\right)\right)$	flow in the ξ direction due to the ξ gradient in perturbed electrostatic pressure
9	$-\frac{3}{2}\mathrm{Co}\varepsilon(\varepsilon-1) \frac{\partial}{\partial \xi}\left[h_0^2 \left(\frac{dc_{5,0}^2}{d\xi}\right) g\right]$	flow in the ξ direction due to the ξ gradient in base-state electrostatic pressure
10	$-q^2 \mathrm{Co}\varepsilon(\varepsilon-1)^2 c_{5,0}^3 g$	flow in the y direction due to the y gradient in perturbed electrostatic pressure
11	$-\frac{3}{2}\mathrm{Ma}\frac{\partial}{\partial \xi}\left(2h_0 \frac{dT_0}{d\xi} g\right)$	flow in the y direction due to the y gradient in base-state temperature field
12	$-\frac{3}{2}\mathrm{Ma}\frac{\partial}{\partial \xi}\left(h_0^2 \frac{\partial T_1}{\partial \xi}\right)$	flow in the ξ direction due to the ξ gradient in perturbed temperature field
13	$\frac{3}{2}\mathrm{Ma}q^2 h_0^2 T_1$	flow in the y direction due to the y gradient in perturbed temperature field

the electric field (multiplied by Co), and three which result from the temperature field (multiplied by Ma).

The mechanical energy associated with the perturbation g of the capillary ridge is given by

$$E = \frac{1}{2} \int_{-\infty}^{\infty} g^2 d\xi = \frac{1}{2}\langle g^2 \rangle. \tag{47}$$

We can rewrite Eq. (44) in a more compact form as

$$\frac{\partial g}{\partial t} = -L[g] \tag{48}$$

and take the inner product of Eq. (48) with g to obtain

$$\frac{\partial}{\partial t}\langle g^2 \rangle = 2\frac{\partial E}{\partial t} = \langle -L[g], g \rangle. \tag{49}$$

Assuming an exponential dependence on time of g implies that $\partial g/\partial t = \sigma g$ and thus

$$\sigma = \frac{\langle g, -L[g] \rangle}{\langle g, g \rangle}. \tag{50}$$

We can now individually examine the contribution of each of the 13 terms of L to the growth rate σ over a range of q. It follows that at a given q, the sum of the 13 terms equals σ. These terms are listed and described in Table I. The first seven terms are identical to those listed in Ref. [3], while terms 8–10 result from the electric field and terms 11–13 come from the temperature gradient. Any term that is negative indicates that it has a stabilizing effect on the perturbation, while positive terms have a destabilizing effect.
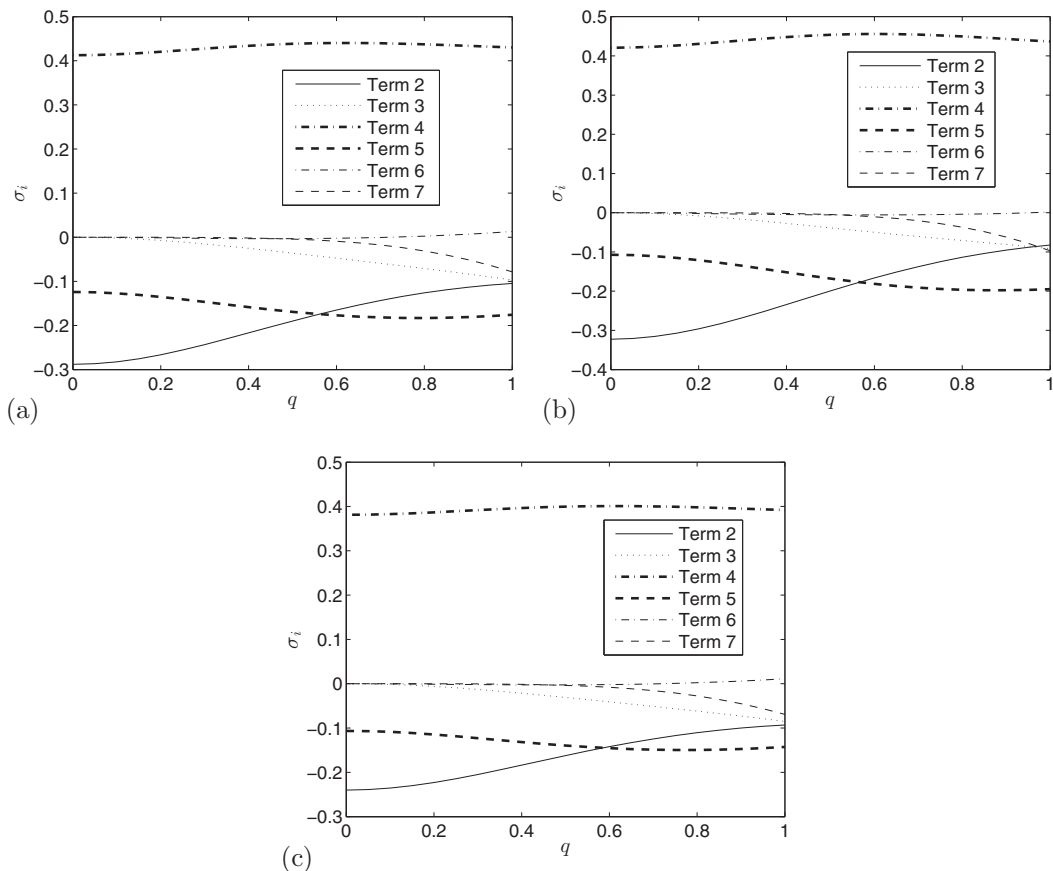
FIG. 5. Contributions to the growth rate from each of the first seven terms of operator L: (a) terms with no electric or temperature field, (b) terms in the presence of only an electric field (Co = 0.2), and (c) terms in the presence of only a temperature field (Ma = 0.1). The values of the other parameters are $\varepsilon = 2.5$ and $\kappa = 5$.

We begin by examining the effects of the electric field on the first seven terms in Table I. These are the standard terms that are present even in the absence of electric and temperature fields. Figure 5(a) shows each term plotted against q when the only external force present is gravity; the behavior is similar to that shown in Fig. 13 of Ref. [3] (term 1 is neglected because it is uniformly 0). Like with Fig. 4, the quantitative differences between this study and that of Spaid and Homsy [3] arise from the difference in initial condition for $h(\xi, t = 0)$. Figure 5(b) shows those same terms when an electric field is present, with the strength of the electric field taken as Co = 0.2. Other values of Co can be chosen, and although the precise values of the curves for each term will be different, the trends that we discuss below are largely the same.

As will be discussed below, close inspection of Figs. 5(a) and 5(b) reveals that, in general, the electric field has a destabilizing effect on the standard terms. This might be expected given that these terms represent the behavior of the perturbation g in response to the traveling-wave profile of h_0; the higher capillary ridge should result in a larger contribution to the growth rate from these terms. At q lower than approximately 0.5, terms 5 and 4 are affected the most by the electric field. We see that term 5 in Fig. 5(b), although still negative, is not as strongly stabilizing as when the electric field is absent. Term 4, representing flow in the ξ direction due to gravity, actually has a slightly greater value when an electric field is present.
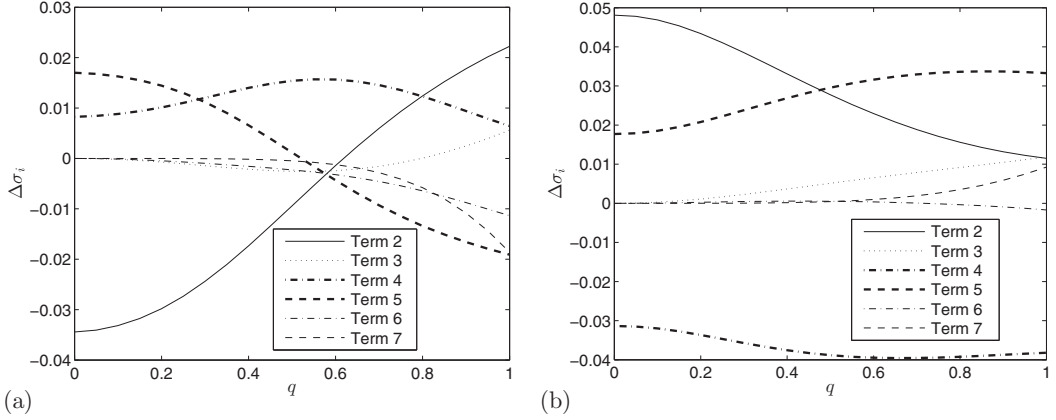
FIG. 6. (a) Difference in growth rate between each standard term with Co = 0.2 and Co = 0 with $\varepsilon = 2.5$. (b) Difference in growth rate between each standard term with Ma = 0.1 and Ma = 0 with $\kappa = 5$.

We can get a more quantitative picture of how the electric field affects each physical mechanism by plotting the difference between each term with and without an electric field across the spectrum of q. In Fig. 6(a) we see that for smaller values of q, terms 4 and 5 show an increase as a consequence of the electric field, whereas term 2 is stabilizing. For larger values of q only terms 2–4 are destabilized by the electric field.

In general, the electric field acts on the perturbation in two distinct ways. First, as we just described, it destabilizes the front implicitly through its impact on the capillary ridge, as demonstrated by examining the standard terms of L [Figs. 5(a) and 5(b)]. Second, the electric field may act directly on the perturbation to destabilize it to generate the increased growth rates shown in Fig. 4(a). This corresponds to the additional terms in the operator L that are multiplied by Co.

We now turn to examining these additional terms. Figure 7(a) shows the contributions to the growth rate from terms 8–10 introduced by the electric field. Terms 8 and 10 are positive, whereas term 9 is negative, over the range of q shown. Terms 8 and 9, resulting from ξ curvature in the perturbed and base-state electrostatic pressure, respectively, are relatively balanced. Term 10, arising from y curvature of the perturbed electrostatic pressure field, scales as q^2 and rapidly destabilizes
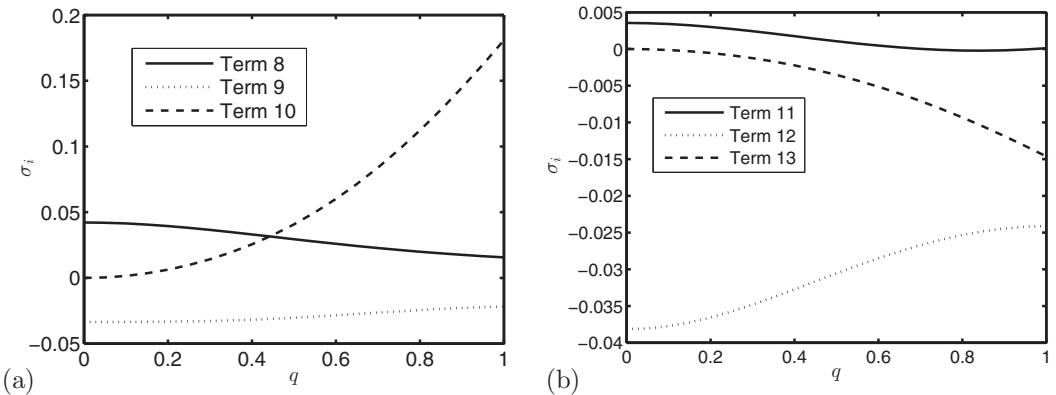

FIG. 7. Energy analysis results for (a) Co = 0.2 and $\varepsilon = 2.5$ (Ma = 0) and (b) Ma = 0.1 and $\kappa = 5$ (Co = 0).

the film front as q increases. When the contributions from terms 8–10 are included, the net effect of the electric field is to increase the overall growth rates of the spanwise perturbations.

To examine the effects of thermocapillarity on the standard terms, we compare Fig. 5(a) to Fig. 5(c). Term 4 is now slightly more stabilizing relative to the case with no temperature and electric field. This might be expected as term 4 is the contribution from gravity acting on the film, and this action is reduced due to the smaller size of the capillary ridge. We see that term 2, originating from the curvature of the perturbed height profile, is significantly less stabilizing than it is in the case with no temperature field. The difference between each standard term at Ma = 0.1 and Ma = 0 is shown in Fig. 6(b). From this plot we can see that the differences between most terms follow the same trends as they do in Fig. 6(a). Overall, the contribution to the growth rate from terms 1–7 is slightly increased at low q, but rapidly decreases at $q > 0.6$ mainly due to terms 2 and 4. The rest of the stabilization is due to thermocapillary effects acting directly on the perturbed height profile, as evidenced by terms 11–13 and discussed below.

We plot the effects of terms 11–13 across a range of wave numbers in Fig. 7(b). Here we see mixed contributions from the interfacial temperature gradient, with term 11 destabilizing the perturbation and terms 12 and 13 acting as stabilizing influences. Term 11 is a result of the ξ curvature of the base-state temperature field, while terms 12 and 13 both come from curvature of the perturbed temperature field. At low q, there is negligible y curvature in the perturbed temperature field, so term 13 is also negligible. Thus, term 12, arising from ξ curvature of the perturbed temperature field, is the dominant stabilizing mechanism until $q \approx 1$. Interestingly, term 11, which arises from the base-state temperature field, is approximately constant across the range of q shown, consistent with the fact that the base-state temperature field is independent of q.

We now offer additional physical explanations for the effects that electric and temperature fields have on the stability of the film front. By supposing a sinusoidal form of the disturbance $g(\xi, t)$, the perturbation to $h_0(\xi)$ generates alternating thick and thin regions of liquid in the y direction. Spaid and Homsy [3] postulate two possible explanations for why fingers result from this alternating thickness profile. First, the thicker regions are more massive and thus are pushed forward more rapidly by the body force. Second, the thicker regions are less affected by viscous drag, increasing the mobility in these regions of the film. Either way, faster growth of $g(\xi, t)$ increases the height disparity between the thick and thin regions of the liquid and will result in earlier onset of the fingering instability.

In Fig. 8 we plot the traveling-wave solution $h_0(\xi)$ and corresponding eigenfunction $g(\xi, t)$ of the operator L with $q = 0.5$ in the presence of no electric or temperature field [Fig. 8(a)], an electric field (Co = 0.2) [Fig. 8(b)], and a temperature field (Ma = 0.1) [Fig. 8(c)]. In each case, the nonzero region of the eigenfunction develops in the same region of the domain as the *leading face* of the capillary ridge. The growth rate σ is calculated from the L^2-norm of $g(\xi, t)$, and because $g(\xi, t)$ is zero everywhere except on the leading face of the capillary ridge, its growth in this region determines the growth rate of the instability.

To understand the role the electric field plays in enhancing the growth of the instability, recall the distribution of the electrostatic pressure in the traveling-wave solution to Eq. (27). Figure 2(b) shows that there is a minimum in electrostatic pressure located directly on the capillary ridge which increases its height by pumping liquid from the surrounding areas. One of the regions to which the base-state electrostatic pressure pumps liquid is the leading face of the capillary ridge, i.e., the region most critical to the growth of $g(\xi, t)$. This action of the base-state electrostatic pressure enhances the ability of $g(\xi, t)$ to grow in that region and results in the increase in terms 8 and 10. Thus, the electric field increases the growth rate of the instability [Fig. 4(a)].

The eigenfunction $g(\xi, t)$ and base state $h_0(\xi)$ for the case of thermocapillary stabilization are shown in Fig. 8(c). Once again the nonzero part of $g(\xi, t)$ develops on the leading face of the capillary ridge. In this case thermocapillary forces from the base-state temperature gradient pump liquid down from the peak of the capillary ridge into the region where $g(\xi, t)$ is nonzero (i.e., from the hotter region with lower surface tension to the cooler regions with higher surface tension). This base-state thermocapillary flow encourages the growth of $g(\xi, t)$ and causes term 11 to be positive,
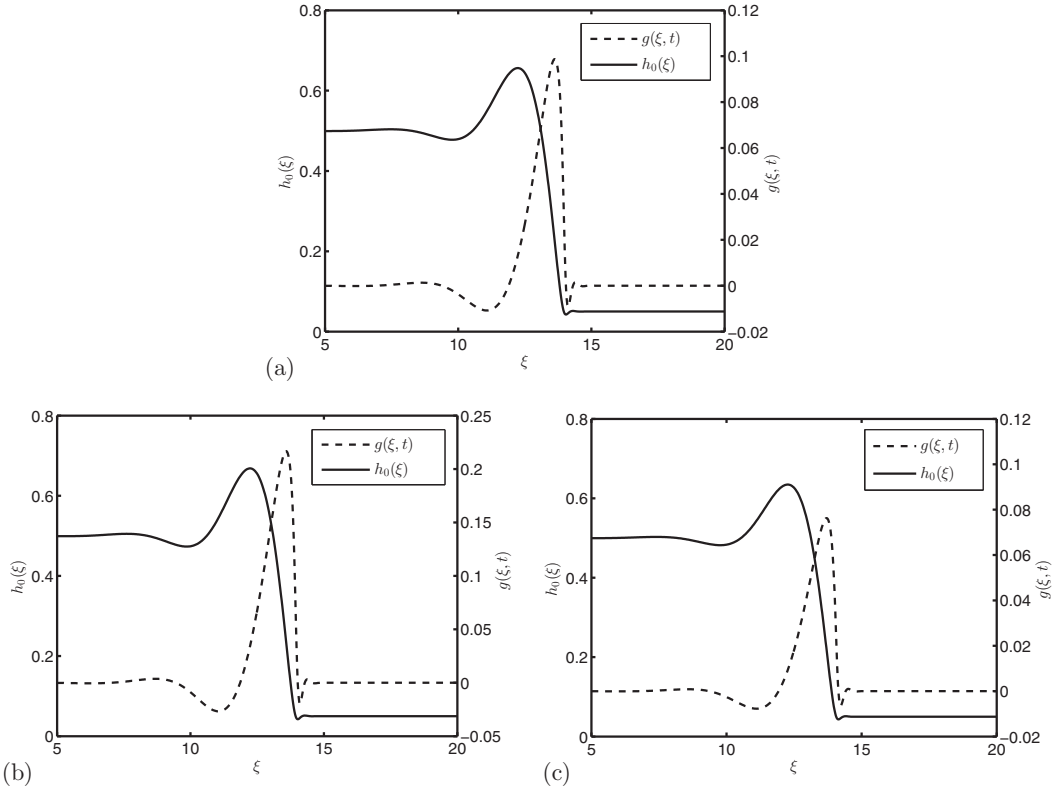
FIG. 8. Eigenfunctions of the operator $L(q = 0.5)$ overlaid with base states for (a) Co = 0 and Ma = 0, (b) Co = 0.2 and $\varepsilon = 2.5$ (Ma = 0), and (c) Ma = 0.1 and $\kappa = 5$ (Co = 0).

thus increasing the growth rate [see Fig. 7(b)]. However, we also see in Fig. 7(b) that terms 12 and 13, which arise due to gradients in the perturbed temperature field, are strongly stabilizing. This is because thermocapillary stresses in the height perturbation drive liquid out of the hotter peaks and into the cooler valleys of $g(\xi, t)$, flattening the perturbation and slowing the growth of $g(\xi, t)$.
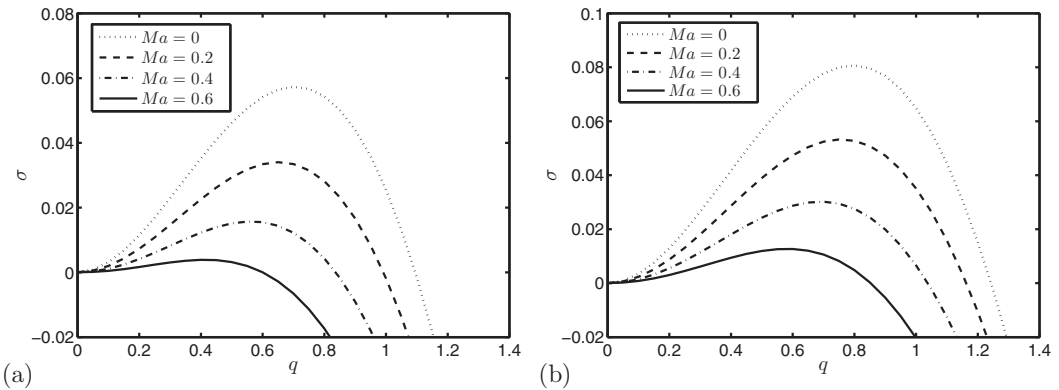

FIG. 9. Dispersion relations showing thermocapillary stabilization and electrohydrodynamic destabilization for various values of Ma. The parameter values are $\varepsilon = 2.5$, $\kappa = 5$, and (a) Co = 0.05 and (b) Co = 0.1.

We see that the combined stabilization from terms 12 and 13 outweighs the destabilizing effect of term 11, thus generating the overall diminished growth rates seen in Fig. 4(b) for Ma > 0.

Since the electrohydrodynamic effects are destabilizing, it is of interest to explore the extent to which thermocapillary forces can be used counteract this. Such combined fields may be of interest in practical applications where electric fields are present and temperature gradients can be applied. In Fig. 9 we plot the dispersion relation as a function of Ma for two different values of Co. For Co = 0.05 [Fig. 9(a)] we see that a value of approximately Ma = 0.6 is needed to bring the dispersion relation close to neutral stability. For larger Co the growth rates increase [Fig. 9(b)], however doubling Co increases the growth rates by much less than a factor of 2.

VI. CONCLUSION

In this paper we have examined the effects of electric and temperature fields on the linear stability of gravity-driven thin liquid films with contact lines. We considered a perfect dielectric liquid with surface tension that decreases linearly with increasing temperature. Using lubrication theory, an evolution equation for the film thickness was derived which predicted the existence of traveling-wave liquid profiles in the presence of both electric and temperature fields. We found that the electric field always acts to increase the height of the capillary ridge of the traveling-wave profile, which increases both the growth rate and most unstable wave number of the instability. A temperature field can either increase (when Ma < 0) or decrease (when Ma > 0) the height of the capillary ridge of the traveling-wave profile, depending on the direction of the temperature gradient.

An energy analysis was performed to gain insight into the physical mechanisms behind the effects that electric and temperature fields have on the linear stability of driven films. In the case of electric fields, it was determined that the base-state electrostatic pressure was the dominant force responsible for destabilization of the film front. With temperature fields such that Ma > 0, the dominant stabilizing mechanisms were from the gradients in the perturbed temperature field. In both the cases of electric and temperature fields, it was found that these external forces impact contact-line stability not only through their influence on the capillary ridge, but also through the perturbed profiles of the interface height. We note that because of the complex coupling between the base-state quantities and the perturbation variables, the calculations presented here are needed to definitively ascertain the effects of electric fields and temperature gradients on contact-line stability.

In practical situations where electrostatic effects are present, they would have a destabilizing effect but could be counteracted by applying a suitable temperature gradient. Because our analysis was focused mainly on regimes where perturbation growth rates are positive, transient amplification was not considered [34]. It is possible that in situations where the growth rates are significantly damped by the temperature field, transient amplification of disturbances may become important. A transient analysis and three-dimensional nonlinear simulations would be helpful toward developing a more complete understanding of electrohydrodynamic and thermocapillary effects on the fingering instability in gravity-driven spreading films.

ACKNOWLEDGMENTS

---

[1] B. Preinerstorfer, M. Lämmerhofer, and W. Lindner, Advances in enantioselective separations using electromigration capillary techniques, Electrophoresis **30**, 100 (2009).

[2] H. Hansen, Method for spray-coating medical devices, US Patent No. 6,669,980 (30 December 2003).

[3] M. A. Spaid and G. M. Homsy, Stability of Newtonian and viscoelastic dynamic contact lines, Phys. Fluids **8**, 460 (1996).

[4] A. L. Bertozzi and M. P. Brenner, Linear stability and transient growth in driven contact lines, Phys. Fluids **9**, 530 (1997).

[5] L. Kondic and J. Diez, Pattern formation in the flow of thin films down an incline: Constant flux configuration, Phys. Fluids **13**, 3168 (2001).

[6] S. M. Troian, E. Herbolzeimer, S. A. Safran, and J. F. Joanny, Fingering instabilities of driven spreading films, Europhys. Lett. **10**, 25 (1989).

[7] R. V. Craster and O. K. Matar, Dynamics and stability of thin liquid films, Rev. Mod. Phys. **81**, 1131 (2009).

[8] R. A. Hayes and B. J. Feenstra, Video-speed electronic paper based on electrowetting, Nature (London) **425**, 383 (2003).

[9] F. Mugele and J.-C. Baret, Electrowetting: From basics to applications, J. Phys.: Condens. Matter **17**, R705 (2005).

[10] M. Mohammadi, H. Madadi, and J. Casals-Terré, Microfluidic point-of-care blood panel based on a novel technique: Reversible electroosmotic flow, Biomicrofluidics **9**, 054106 (2015).

[11] J. M. Davis and S. M. Troian, Influence of attractive van der Waals interactions on the optimal excitations in thermocapillary-driven spreading, Phys. Rev. E **67**, 016308 (2003).

[12] A. Corbett and S. Kumar, Combined thermal and electrohydrodynamic patterning of thin liquid films, J. Eng. Math. **94**, 81 (2015).

[13] O. V. Salata, Tools of nanotechnology: Electrospray, Curr. Nanosci. **1**, 25 (2005).

[14] D. E. Kataoka and S. M. Troian, A theoretical study of instabilities at the advancing front of thermally driven coating films, J. Colloid Interface Sci. **192**, 350 (1997).

[15] J. Klentzman and V. S. Ajaev, The effect of evaporation on fingering instabilities, Phys. Fluids **21**, 122101 (2009).

[16] A. Corbett and S. Kumar, Spreading of thin droplets of perfect and leaky dielectric liquids on inclined surfaces, Langmuir **32**, 6606 (2016).

[17] A. Oron, S. H. Davis, and S. G. Bankoff, Long-scale evolution of thin liquid films, Rev. Mod. Phys. **69**, 931 (1997).

[18] J. P. Singer, Thermocapillary approaches to the deliberate patterning of polymers, J. Polym. Sci. B **55**, 1649 (2017).

[19] T. Gambaryan-Roisman, Modulation of Marangoni convection in liquid films, Adv. Colloid Interface Sci. **222**, 319 (2015).

[20] D. T. Papageorgiou, Film flows in the presence of electric fields, Annu. Rev. Fluid Mech. **51**, 155 (2019).

[21] L. Chen and E. Bonaccurso, Electrowetting—From statics to dynamics, Adv. Colloid Interface Sci. **210**, 2 (2014).

[22] D. Tseluiko, M. G. Blyth, D. T. Papageorgiou, and J.-M. Vanden-Broeck, Electrified viscous thin film flow over topography, J. Fluid Mech. **597**, 449 (2008).

[23] D. Tseluiko, M. G. Blyth, D. T. Papageorgiou, and J.-M. Vanden-Broeck, Electrified film flow over step topography at zero Reynolds number: An analytical and computational study, J. Eng. Math. **69**, 169 (2011).

[24] D. A. Saville, Electrohydrodynamics: The Taylor-Melcher leaky dielectric model, Annu. Rev. Fluid Mech. **29**, 27 (1997).

[25] M. Dietzel and S. M. Troian, Formation of Nanopillar Arrays in Ultrathin Viscous Films: The Critical Role of Thermocapillary Stresses, Phys. Rev. Lett. **103**, 074501 (2009).

[26] M. Dietzel and S. M. Troian, Mechanism for spontaneous growth of nanopillar arrays in ultrathin films subject to a thermal gradient, J. Appl. Phys. **108**, 074308 (2010).

[27] J. A. Moriarty, L. W. Schwartz, and E. O. Tuck, Unsteady spreading of thin liquid films with small surface tension, Phys. Fluids A **3**, 733 (1991).

[28] M. H. Eres, L. W. Schwartz, and R. V. Roy, Fingering phenomena for driven coating films, Phys. Fluids **12**, 1278 (2000).

[29] L. W. Schwartz, D. Roux, and J. J. Cooper-White, On the shapes of droplets that are sliding on a vertical wall, Physica D **209**, 236 (2005).

[30] R. Goodwin and G. M. Homsy, Viscous flow down a slope in the vicinity of a contact line, Phys. Fluids A **3**, 515 (1991).

[31] L. Kondic, Instabilities in gravity driven flow of thin fluid films, SIAM Rev. **45**, 95 (2003).

[32] L. Espín and S. Kumar, Forced spreading of films and droplets of colloidal suspensions, J. Fluid Mech. **742**, 495 (2014).

[33] N. Tiwari, Z. Mester, and J. M. Davis, Stability and transient dynamics of thin liquid films flowing over locally heated surfaces, Phys. Rev. E **76**, 056306 (2007).

[34] R. O. Grigoriev, Transient growth in driven contact lines, Physica D **209**, 105 (2005).